

CrystEngComm

Accepted Manuscript



This is an *Accepted Manuscript*, which has been through the Royal Society of Chemistry peer review process and has been accepted for publication.

Accepted Manuscripts are published online shortly after acceptance, before technical editing, formatting and proof reading. Using this free service, authors can make their results available to the community, in citable form, before we publish the edited article. We will replace this *Accepted Manuscript* with the edited and formatted *Advance Article* as soon as it is available.

You can find more information about *Accepted Manuscripts* in the [Information for Authors](#).

Please note that technical editing may introduce minor changes to the text and/or graphics, which may alter content. The journal's standard [Terms & Conditions](#) and the [Ethical guidelines](#) still apply. In no event shall the Royal Society of Chemistry be held responsible for any errors or omissions in this *Accepted Manuscript* or any consequences arising from the use of any information it contains.

Cite this: DOI: 10.1039/c0xx00000x

www.rsc.org/crystengcomm

PAPER

Mesoporous Nanobelts and Nano-necklace of Co_3O_4 Converted from $\beta\text{-Co(OH)}_2$ Nanobelts via Thermal Decomposition Route for Electrocatalytic Oxidation of H_2O_2

5 **Qiang Wang^{a*}, Yanping Xia^a and Changlong Jiang^b**a. *School of materials science and engineering, Changzhou university, Changzhou, Jiangsu, 213164, P.R.China. E-mail: wq@cczu.edu.cn*b. *Institute of Intelligent Machines, Chinese Academy of Sciences and Department of Chemistry, University of Science & Technology of China, Hefei, Anhui 230026, P.R.China*

10

Received (in XXX, XXX) Xth XXXXXXXXX 20XX, Accepted Xth XXXXXXXXX 20XX

DOI: 10.1039/b000000x

We developed a direct and scalable approach, based upon a thermal decomposition approach under normal atmospheric pressure for growing well-defined mesoporous Co_3O_4 nanobelts and nano-necklaces from the uniform precursor $\beta\text{-Co(OH)}_2$ nanobelts. This method involves the synthesis of the precursors via a solution process and subsequently thermal decomposition of the precursors at atmospheric pressure. The operation is quite simple and environmentally benign, with no release of gas pollutants and no need of protective inert gas during the synthesis. And the final morphologies of products can be easily tuned by modifying the heating temperature and the heating rate. Due to its high specific area and porous structure, the spine Co_3O_4 mesoporous nanobelts exhibit enhanced electrocatalytic oxidation performance in comparison with Co_3O_4 nano-necklaces toward hydrogen peroxide under the alkaline electrolyte.

1. Introduction

The development and innovation of strategies for the fabrication of nanostructured materials has been among the hot research topics in the field of nanoscience, not only for the significant scientific importance in understanding the thermodynamics and kinetics process of nanocrystal growth, but also for the novel properties of these nanomaterials that differ drastically from their bulk counterparts and their potential applications in many areas including chemical, physical, biological and engineering fields.¹⁻⁸ It is well known that the chemical compositions, polymorphs, and morphologies—such as crystalline sizes, shapes, orientations, and assemblies, which are related to the preparation methodology, would have a significant influence on the performances of as-prepared nanocrystals.⁹⁻¹⁵ In order to develop new functional materials with improved performance, the rational design and preparation of nanostructured materials has been continuously pursued.

Spinel Co_3O_4 is an important magnetic p-type semiconductor with the normal spinel structure denoted as AB_2O_4 . Due to its much intriguing magnetic, optical, electronic, and electrochemical properties, Co_3O_4 has attracted considerable attention from many researchers in the past few years and presents broad practical applications in several important technological fields, including heterogeneous catalysts, anode materials in Li-ion rechargeable

batteries, solid-state sensors, optical devices, solar energy absorbers, and magnetic materials. Porous Co_3O_4 nanostructures, with a higher surface area and abundant transporting channels, is especially attractive for optimizing properties and enhancing performance.¹⁶⁻²⁷ Up to now, many synthesis approaches have been recently developed, for example, sol-gel, spray pyrolysis, thermal decomposition, microemulsion, and solvothermal growth. Co_3O_4 nanocrystals with various morphologies, such as nanotubes, nanorods, nanosheets, hollow nanospheres and nanocages, have been prepared.²⁸⁻³²

Herein, we introduce a direct and scalable approach, based upon a thermal decomposition approach under normal atmospheric pressure via a precursor-induced mechanism, for growing well-defined mesoporous Co_3O_4 nanobelts and nano-necklaces from the uniform precursor $\beta\text{-Co(OH)}_2$ nanobelts. The typical synthesis of the current strategy is based on the thermal decomposition of the precursor $\beta\text{-Co(OH)}_2$ nanobelts from room temperature to fixed heating temperature at a suitable heating rate. This method involves the synthesis of the precursor via a solution process and subsequently thermal decomposition of the precursor at atmospheric pressure. The operation is quite simple and environmentally friendly, with no release of gas pollutants and no need of protective inert gas during the synthesis. Also, this method is effective for the synthesis of Co_3O_4 nanocrystals on a gram scale, and the final morphologies can be easily tuned by

modifying the heating temperature and the heating rate. This synthetic strategy might not only shed a new light on the facile, general synthesis and functional mechanisms of the functional metal oxide nanobelts, but also extend the practical applications of the nanobelts in a variety of fields.

2. Experimental section

2.1 Chemicals and Materials

All the reagents used in this work, including $\text{CoCl}_2 \cdot 6\text{H}_2\text{O}$, urea, sodium hydroxide, hydrogen peroxide and ethanol were purchased from Sigma-Aldrich and were of analytical grade and used as received without further purification. Deionized water (18.2 M Ω) was obtained from a Millipore Milli-Q purification system.

2.2 Synthesis of the $\beta\text{-Co(OH)}_2$ Nanobelts

In a typical experiment, $\text{CoCl}_2 \cdot 6\text{H}_2\text{O}$ (0.1 g) and urea (0.6 g) were mixed in 10 mL deionized water to give a solution, and the obtained mixture was heated at 95 °C for 12 h under magnetic stirring in air. Upon cooling the resulting precipitate was collected by filtration, washed with distilled water for several times, and further dried at 50 °C in air to yield the products.

2.3 Synthesis of the mesoporous Co_3O_4 Nanobelts

In a typical synthesis of the precursors, the as-synthesized $\beta\text{-Co(OH)}_2$ nanobelts were placed into an alumina boat (70 mm x 14 mm x 10 mm). The alumina boat was heated in a furnace to 300 °C at a rate of 2 °C min⁻¹ and subsequently annealed at fixed temperature (300 °C) for 90 min under atmospheric pressure, and then the sample was collected for further characterization.

2.4 Synthesis of the Co_3O_4 Nano-necklaces

The as-synthesized $\beta\text{-Co(OH)}_2$ nanobelts were placed into an alumina boat (70 mm x 14 mm x 10 mm). The alumina boat was heated in a furnace to 700 °C at a rate of 2 °C min⁻¹ and subsequently annealed at fixed temperature (700 °C) for 90 min under atmospheric pressure, and then the sample was collected for further characterization.

2.5 Characterization

The field-emission scanning electron microscope (FE-SEM) images were obtained using a JEOL JSM 6701 microscope, operating at 10 A and 5 kV. The transmission electron microscope (TEM) experiment was performed with a JEOL 3010 system by mounting the sample on a carbon-coated copper grid. The crystallographic phase of the sample was determined by powder XRD on a Siemens D5005 X-ray diffractometer with Cu K α radiation ($\lambda = 1.5406 \text{ \AA}$) at a scan rate of 0.01 °/s at 40 kV/40mA in the 2θ range from 10 ° to 70 °. The adsorption isotherm of N_2 on the samples was measured at 77 K using Autosorb iQ Station2. Prior to measuring the adsorption isotherm, the samples were outgassed at 150 °C for 10 hours. The specific surface area was calculated by multipoint BET method, the pore size was based on adsorption Barrett–Joiner–Halenda (BJH) method.

To modify the electrode surface, an aliquot of 5 mL of 1 mg/mL as-synthesized Co_3O_4 powder suspension of water after

sonification for 5 minutes was pipetted onto the glassy carbon electrode (GCE) surface and dried in air.

Electrochemical measurements were performed on a CHI 660B electrochemical workstation (CHI Instruments, USA). All experiments were carried out with a three-electrode system with a glassy carbon electrode ($\varnothing = 3 \text{ mm}$) as the working electrode, a platinum wire as the auxiliary electrode and a saturated calomel electrode (SCE) as reference electrode. 0.1M NaOH solution was used as the supporting electrolyte.

3. Results and discussion

Metal oxides, as an important class of functional materials, have been intensively probed in the past few decades because of their unique size-dependent electrical, optical and magnetic properties, which are expected to find useful applications in lithium-ion batteries, magnetic storages, catalysis and sensors, *etc.* Many methods had been developed for the synthesis of metal oxide nanocrystals.³³⁻³⁴ Among them, the most successful is the thermolysis of various organometallic precursors in complex organic solvent systems.³⁵ In addition, thermal decomposition based on non-hydrolytic systems has proven to be highly versatile and reliable for the preparation of the nanocrystals,³⁶⁻³⁸ but the shapes of the obtained nanocrystals are mainly spherical, cubic, rodlike and polyhedral. Since the successful synthesis of oxide nanobelts in Wang's lab by thermal evaporation method, the investigation of oxide nanobelts has attracted considerable attention.³⁹⁻⁴¹ However, the thermal evaporation method needs high heating temperature and protective inert gases during the synthetic process. Therefore, exploring and developing a rational, effective and facile synthetic method to fabricate the functional oxide nanobelts on a large scale is necessary and continues to be a key challenge in the field of material synthesis and structure design, which is not only important for fundamental research but also for wider application in practical fields.

In the current synthesis, the Co_3O_4 mesoporous nanobelts and nano-necklaces were fabricated from the precursor $\beta\text{-Co(OH)}_2$ nanobelts by thermal decomposition route. As shown in figure 1, the precursor $\beta\text{-Co(OH)}_2$ nanobelts were obtained through the solution reaction of $\text{CoCl}_2 \cdot 6\text{H}_2\text{O}$ with urea in aqueous solution at mild experimental condition. When heated the precursor nanobelts at temperature of 300 °C, the $\beta\text{-Co(OH)}_2$ precursor can be decomposed into Co_3O_4 and H_2O (gas phase), and the instantaneous formed gaseous water during the process might release from the surface of the nanobelts and leave porous structures in the nanobelts, resulting into the formation of the Co_3O_4 mesoporous nanobelts. When treated the precursor nanobelts at higher temperature (700 °C), the final sample demonstrated as a novel shape, necklace-like nanocrystals. During the heating progress, the morphology of the precursor will keep stable while the phase transformed into the corresponding dehydrated metal oxide Co_3O_4 nanocrystals, namely, the formation of mesoporous nanobelts and nano-necklaces of Co_3O_4 might be dominated via a precursor-induced mechanism.

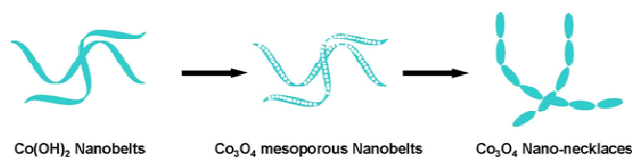


Figure 1. The schematic illustration of Co_3O_4 mesoporous nanobelts and nano-necklaces growth from the precursor via a controllable thermal decomposition route.

Cobalt hydroxides have attracted intense interest due to their many important applications. For example, cobalt hydroxide can be added as a component or additive to improve the electrochemical properties of nickel hydroxide electrodes, alkaline secondary batteries and $\beta\text{-Co(OH)}_2/\text{zeolite}$ molecular sieves.⁴² Moreover, α and $\beta\text{-Co(OH)}_2$ have been investigated to use as reactive templates for highly textured thermoelectric cobaltite ceramics and as the precursor for the preparation of cobalt oxides nanomaterials by the thermal conversion following topotactic formation mechanism.⁴³⁻⁴⁴

The precursor was obtained through the solution reaction of $\text{CoCl}_2 \cdot 6\text{H}_2\text{O}$ with urea in aqueous solution at mild experimental condition. The phase structure and crystalline of the precursor and annealing products were firstly examined by X-ray diffraction (XRD) studies, the peaks in the patterns of the precursor (Figure S1a) can be indexed to pure hexagonal phase of cobalt hydroxide $\beta\text{-Co(OH)}_2$ (Joint Committee on Powder Diffraction Standards (JCPDS) card no. 30-443), the XRD pattern of the samples after heating the precursor matches very well with that of cubic spinel Co_3O_4 (JCPDS card no. 42-1467), and the result shows that the products have good crystallinity as proved by the XRD measurements (Figure S1b and c).

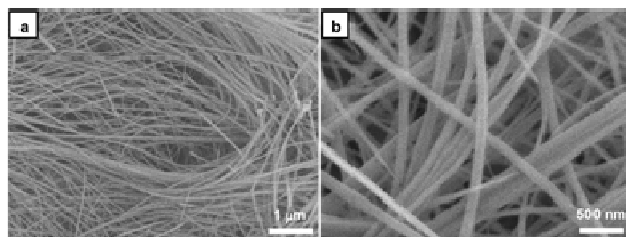


Figure 2. FE-SEM images of the $\beta\text{-Co(OH)}_2$ nanostructures. (a) Low magnification and (b) high magnification SEM images of the nanobelts.

The morphology of the samples was then characterized by field emission scanning electron microscopy (FESEM). The typical SEM image (Figure 2a) of the obtained precursor shows primarily belt-like structures with a lateral size ranging from 100 to 200 nm and length of several tens of micrometers. Figure 2b shows the high-magnification SEM image of as-prepared precursor nanobelts with remarkably smooth surface morphology and a thickness of about 15 nm. Transmission electron microscopy (TEM) images recorded on the precursor nanobelts provide further insight into the structure of the products. Figure S2a clearly shows belt-like structures of the obtained samples, and the corresponding selected area electron diffraction (SAED) pattern (Figure S2c) of the nanobelts also confirms the single crystalline essence of the $\beta\text{-Co(OH)}_2$ nanobelts. The HRTEM images (Figure S2d) further verifies the single-crystalline nature

of the nanobelts and the absence of line or planar defects. The lattice constant of the $\beta\text{-Co(OH)}_2$ nanobelts was calculated to be 4.61 Å, also consistent with the interplanar separation between the (001) plane of $\beta\text{-Co(OH)}_2$ crystal.

After heating the precursors at fixed temperature (300 °C), the precursor nanobelts will transform into the corresponding metal oxide Co_3O_4 , as shown in Figure 3. When annealed the precursor nanobelts, the precursor will be decomposed into Co_3O_4 and gaseous water, and the obtained Co_3O_4 samples still remain the belt-like morphology similar to the precursor (Figure 3a), which has a lateral size ranging from 100 to 200 nm and length of several tens of micrometers. The high magnification FESEM images (Figure 3b) clearly demonstrated uniform nanobelts with density nanopores in the nanobelts, and the mesoporous nanobelts have well-distributed nanopores with the size of several nm. TEM measurements were further performed for the as-obtained Co_3O_4 samples, and the low-magnification TEM image (Figure 3c) clearly shows the Co_3O_4 samples are uniform nanobelts with the lateral size ranging from 100 to 200 nm, which has a lot of well-defined nanopores on the surface. HRTEM observation (Figure 3d) further verifies the mesoporous nature of the nanobelts and the SAED pattern (inserted in Figure 3b) exhibits the polycrystalline nature of the mesoporous Co_3O_4 nanobelts, resulting from the porous texture of the nanobelts. The BET specific surface area and the average pore diameter were 79.548 m^2/g and 19.93 nm, respectively that is consistent with TEM observation (Figure S5).

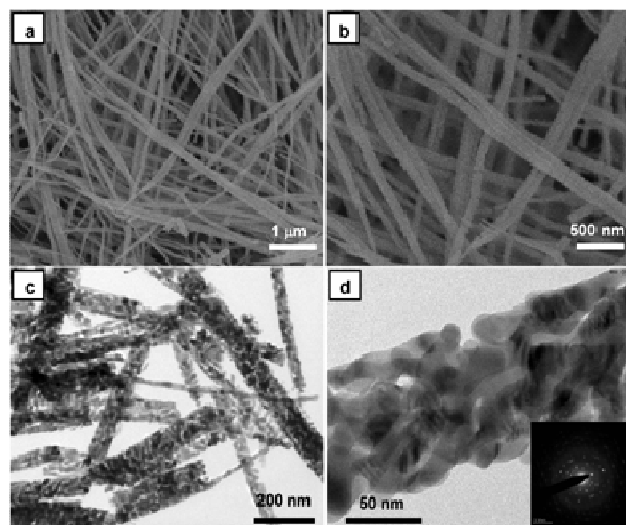


Figure 3. FE-SEM and TEM images of the Co_3O_4 nanostructures synthesized at 300 °C. (a) low magnification and (b) high magnification SEM images of the Co_3O_4 mesoporous nanobelts; (c) low magnification and (d) high magnification TEM images of the Co_3O_4 mesoporous nanobelts, inserted (d) is the SAED pattern of the mesoporous nanobelts.

The reaction temperature might play a vital role in the shape evolution of the resulted samples. In current synthesis, when treated the precursor nanobelts at higher temperature (700 °C), the obtained products did not demonstrate porous nanobelts but an interesting morphology – necklace-like nanocrystals. Figure 4a is the low-magnification SEM image of the obtained nano-necklaces, which has a lateral size ranging from 100 to 200 nm and length of several tens of micrometers. The high magnification

FESEM images (Figure 4b and c) clearly show the necklace-like shape of the obtained samples, and all the necklaces were consisted of small short blocks linked each other. Figure 4d presents the high magnification FESEM image of a single nano-necklace, which has small short blocks linked along the nanocrystals. TEM measurements were further performed for the as-obtained necklace-like nanocrystals, and the low-magnification TEM image (Figure S3a and S3b) clearly demonstrates the Co_3O_4 samples are the nano-necklaces with uniform size and the length of about several tens of micrometers and the BET specific surface area of this sample is only $11.18 \text{ m}^2/\text{g}$ which matches well with that no inner pores can be detected in the nanobelts. Figure S3c is the high magnification TEM image of a single Co_3O_4 nano-necklace, which is consisted of small short blocks with smooth surface linked each other. The above observation can not be explained by Ostwald ripening process for no hollow structure or large pores presence. Since the melting point of bulk Co_3O_4 is around $900 \text{ }^\circ\text{C}$ in air, high temperature ($700 \text{ }^\circ\text{C}$) may induce nanosized Co_3O_4 grains melting locally and deforming to destroy the original porous frame. The SAED pattern (Figure S3d) confirms the polycrystalline nature of the Co_3O_4 nano-necklaces.

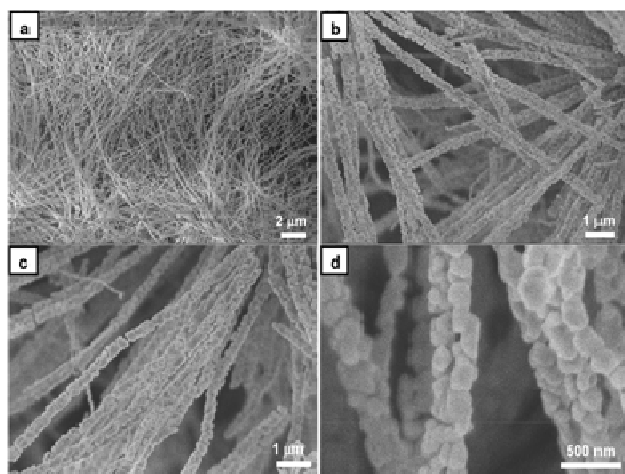
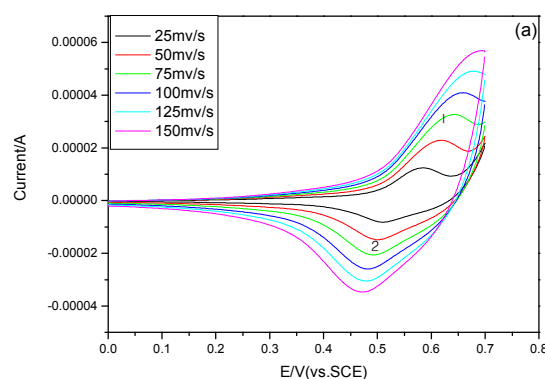


Figure 4. FE-SEM images of the Co_3O_4 nano-necklaces synthesized at $700 \text{ }^\circ\text{C}$. Low magnification (a) and high magnification (b, c and d) SEM images of the Co_3O_4 nano-necklaces.

As mentioned above, the $\beta\text{-Co}(\text{OH})_2$ precursor decomposed into Co_3O_4 and gaseous water upon the heating treatment, and the related experiments indicated the morphologies can be tuned by adjusting the heating temperature. When set the temperature at $500 \text{ }^\circ\text{C}$, the obtained Co_3O_4 samples did not exhibit mesoporous nanobelts and necklace-like nanocrystals, but resulted into the notched nanowires (Figure S4a), which have the diameter of about 100 nm with gaps along the nanowires, as shown in the high magnification TEM image (Figure S4b). If performed the heating experiment at higher temperature, the decomposition will be faster than that at lower treating temperature, and the instantaneous gaseous water generated from the precursor will escape and leave porous structures on the resulted samples. After heating treated at $900 \text{ }^\circ\text{C}$, the precursor $\beta\text{-Co}(\text{OH})_2$ nanobelts will transform into crashed and short nanofibers (see Figure S4c and d).

Co_3O_4 had been proved to perform well as H_2O_2 oxidation

catalysts in strong basic solution, for transferring electrons between H_2O_2 and an electrode while enabling regeneration after electron exchanges with H_2O_2 .⁴⁵ In order to verify the electrocatalytic activity of the as-synthesised Co_3O_4 porous belts and necklaces modified GCE for H_2O_2 oxidation under the alkaline condition, the electrochemical experiments were carried out. Figure 5a shows the cyclic voltammetric (CV) curves of the porous Co_3O_4 belts modified GCE in 0.1M NaOH solution at different scan rates. A pair of redox peak is observed (marked with 1 and 2), resulting from the reversible transition between CoOOH and CoO_x . With an increase of the scan rate in the range of $25\text{-}150 \text{ mV/s}$, both of the oxidation and reduction currents of peak (marked 1 and 2) increase linearly. These results suggested that the kinetics of the electrochemistry of porous Co_3O_4 belts was a surface-controlled electron transfer process. Figure 5b presents the CVs in the presence of $1 \text{ mM H}_2\text{O}_2$, recorded at Co_3O_4 nanobelts and nano-necklaces modified GC electrode and the bare GC electrode in 0.1M NaOH solution, respectively. The scan rate is 50 mV/s . Only a small current was observed at the bare GC electrode over most of the potential range. While a dramatic increase of current signal starting from around 0.2V (vs.SCE) and peaked at $0.6\text{V}/0.5\text{V}$ (vs.SCE) toward the positive and negative ends of the potential range was observed when Co_3O_4 porous nanobelts electrode was used. This indicates that Co_3O_4 nanobelts electrode has excellent electrocatalytic properties towards H_2O_2 oxidation and reduction, which may be attributed to the large surface area, excellent accessibility of many nanoscale transport channels, and enhanced electron transfer rate from H_2O_2 to as-synthesized Co_3O_4 nanobelts. In contrast, the CV response peaks of Co_3O_4 nanonecklaces is not remarkable, only a weak and broad peak between 0.2V to 0.7 V (vs.SCE) can be seen.



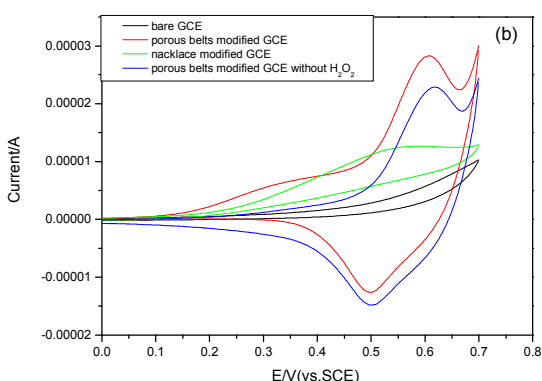


Figure 5. (a) Cyclic voltammograms of the Co_3O_4 nanobelts modified GCE in 0.1M NaOH solution at various scan rates of 25, 50, 75, 100, 125, 150 mV/s. (b) CVs of the Co_3O_4 nanobelts, nano-necklaces modified electrode and the bare GC electrode in 0.1 M NaOH solution in the presence of 1mM H_2O_2 , respectively. Scan rate = 50 mV/s.

4. Conclusion

In conclusion, we have developed a direct and scalable approach, based upon a thermal decomposition approach under normal atmospheric pressure via a precursor-induced mechanism, for growing well-defined mesoporous Co_3O_4 nanobelts and nano-necklaces from the uniform precursor $\beta\text{-Co}(\text{OH})_2$ nanobelts. The remarkable features of this method are that the resulted morphologies of Co_3O_4 nanocrystals can be tuned easily by controlling the heating treatment process during decomposition of the precursors. Due to its high specific area and porous structure, the spine Co_3O_4 mesoporous nanobelts exhibit enhanced electrocatalytic oxidation performance in comparison with Co_3O_4 nano-necklaces toward hydrogen peroxide under the alkaline electrolyte. Furthermore, through this model electrochemical investigation, the produced Co_3O_4 mesoporous nanobelts might be applied in catalyst, sensor and energy storage fields.

Acknowledgements

This work was supported by the Natural Science Foundation of China (Nos. 21371174) and Jiangsu oversea research project of DOE. The authors would like thank Mr F.Q.Zong for providing pores analysis.

Notes and references

† Electronic Supplementary Information (ESI) available: [details of any supplementary information available should be included here]. See DOI: 10.1039/b000000x/

- J. Lee, M. C. Orilall, S. C. Warren, M. Kamperman, F. J. DiSalvo and U. Wiesner, *Nat. Mater.* **2008**, *7*, 222.
- C. L. Jiang, S. J. Liu and Y. B. Han, *CrystEngComm* **2013**, *15*, 7564.
- H. J. Bolink, E. Coronado, J. Orozco, M. Sessolo, *Adv. Mater.* **2009**, *21*, 79.
- J. Park, K. J. An, Y. S. Hwang, J. G. Park, H. J. Noh, J. Y. Kim, J. H. Park, N. M. Hwang and T. Hyeon, *Nat. Mater.* **2004**, *3*, 891.
- C. L. Jiang, R. Y. Liu, G. M. Han and Z. P. Zhang, *Chem. Commun.* **2013**, *49*, 6647.
- Y. Li, W. J. Shen, *Chem. Soc. Rev.* **2014**, *43*, 1543.
- Q. Wang, C. L. Jiang, F. Y. Cao, Q. W. Chen., *J. Nanopart. Res.* **2007**, *9*, 269.

- C. L. Jiang, F. Wang, N. Q. Wu, X. G. Liu, *Adv. Mater.* **2008**, *20*, 4826.
- F. W. Wise, *Acc. Chem. Res.* **2000**, *33*, 773.
- B. Wu, A. Heidelberg and J. J. Boland, *Nat. Mater.* **2005**, *4*, 525.
- X. Duan, Y. Huang, Y. Cui, J. Wang and C. M. Lieber, *Nature* **2001**, *409*, 66.
- M. -J. Lee, S. Han, S. H. Jeon, B. H. Park, B. S. Kang, S. -E. Ahn, K. H. Kim, C. B. Lee, C. J. Kim, I. -K. Yoo, D. H. Seo, X. -S. Li, J. -B. Park, J. -H. Lee and Y. Park, *Nano Lett.* **2009**, *9*, 1476.
- P. M. Rao and X. Zheng, *Nano Lett.* **2009**, *9*, 3001.
- R. S. Devan, R. A. Patil, J. H. Lin and Y. R. Ma, *Adv. Funct. Mater.* **2012**, *22*, 3326.
- J. Andznev, N. Petkov, A. I. Livshits, J. J. Boland, J. D. Holmes and D. Erts, *Nano Lett.* **2009**, *9*, 1824.
- G. Binotto, D. Larcher, A. S. Prakash, R. H. Urbina, M. S. Hegde, J. M. Tarascon, *Chem. Mater.* **2007**, *19*, 3032.
- F. Cheng, Z. Tao, J. Liang, J. Chen, *Chem. Mater.* **2008**, *20*, 667.
- X. W. Lou, D. Deng, J. Y. Lee, L. A. Archer, *J. Mater. Chem.* **2008**, *18*, 4397.
- X. W. Lou, D. Deng, J. Y. Lee, J. Feng, L. A. Archer, *Adv. Mater.* **2008**, *20*, 258.
- H. Zhang, J. B. Wu, C. X. Zhai, X. Y. Ma, N. Du, J. P. Tu, D. R. Yang, *Nanotechnology* **2008**, *19*, 035711.
- Y. G. Li, B. Tan, Y. Y. Wu, *Nano Lett.* **2008**, *8*, 265.
- K. T. Nam, D. W. Kim, P. J. Yoo, C. Y. Chiang, N. Meethong, P. T. Hammond, Y. M. Chiang, A. M. Belcher, *Science* **2006**, *312*, 885.
- L. H. Zhou, J. C. Ge, L. H. Cao, B. Tang, *Cryst. Growth Des.* **2009**, *9*, 1.
- L. H. Hu, Q. Peng, Y. D. Li, *J. Am. Chem. Soc.* **2008**, *130*, 16136.
- J. Li, S. B. Tang, L. Lu, H. C. Zeng, *J. Am. Chem. Soc.* **2007**, *129*, 9401.
- J. Rosen, G. S. Hutchings, F. Jiao, *J. Am. Chem. Soc.* **2013**, *135*, 4516.
- C. Y. Ma, Z. Mu, J. J. Li, Y. G. Jin, J. Cheng, G. Q. Lu, Z. P. Hao, S. Z. Qiao, *J. Am. Chem. Soc.* **2010**, *132*, 2608.
- C. H. Chen, S. F. Abbas, A. Morey, S. Sithambaram, L. P. Xu, H. F. Garces, W. A. Hines, S. L. Suib, *Adv. Mater.* **2008**, *20*, 1205.
- F. Teng, T. Xu, S. Liang, G. Buerger, W. Yao, Y. Zhu, *Cata. Commun.* **2008**, *9*, 1119.
- F. Teng, W. Yao, Y. Zheng, Y. Ma, T. Xu, G. Gao, S. Liang, Y. Teng, Y. Zhu, *Talanta* **2008**, *76*, 1058.
- Y. Z. Shao, J. Sun, L. Gao, *J. Phys. Chem. C* **2009**, *113*, 6566.
- N. Yan, L. Hu, Y. Li, Y. Wang, H. Zhong, X. Y. Hu, X. K. Kong, Q. W. Chen, *J. Phys. Chem. C* **2012**, *116*, 7227.
- X. Wang, J. Zhuang, Q. Peng, Y. D. Li, *Nature* **2005**, *437*, 121.
- A. Narayanaswamy, H. F. Xu, N. Pradhan, X. G. Peng, *Angew. Chem. Int. Ed.* **2006**, *45*, 5361.
- M. Niederberger, G. Garnweitner, *Chem. Eur. J.* **2006**, *12*, 7282.
- D. Kim, J. Park, K. An, N. K. Yang, J. G. Park, T. Hyeon, *J. Am. Chem. Soc.* **2007**, *129*, 5812.
- M. V. Kovalenko, E. Kaufmann, D. Pachinger, J. Roither, M. Huber, J. Stang, G. Hesser, F. Schaffler, W. Heiss, *J. Am. Chem. Soc.* **2006**, *128*, 3516.
- J. E. Murphy, M. C. Beard, A. G. Norman, S. P. Ahrenkiel, J. C. Johnson, P. Yu, O. I. Micic, R. J. Ellingson, A. J. Nozik, *J. Am. Chem. Soc.* **2006**, *128*, 3241.
- Z. W. Pan, Z. R. Dai, Z. L. Wang, *Science* **2001**, *291*, 1947.
- Z. R. Dai, Z. W. Pan, Z. L. Wang, *J. Am. Chem. Soc.* **2002**, *124*, 8673.
- R. Chen, G. Z. Xing, J. Gao, Z. Zhang, T. Wu, H. D. Sun, *Appl. Phys. Lett.* **2009**, *95*, 061908.
- W. Y. Li, S. Zhang, Y. J. Chen, *J. Phys. Chem. B* **2005**, *109*, 14025.
- L. Cao, F. Xu, Y. Y. Liang, H. L. Li, *Adv. Mater.* **2004**, *16*, 1853.
- T. Li, H. L. Zhou, J. X. Fu, X. F. Yang, Y. Wang, H. L. Guo, X. H. Fu, C. L. Liang, M. M. Wu, P. K. Shen, *Adv. Funct. Mater.* **2010**, *20*, 617.
- Y. Ding, Y. Wang, L. Su, M. Bellagamba, H. Zhang, Y. Lei, *Biosensors and Bioelectronics* **2010**, *26*, 542.